ORIGINAL PAPER

Storm surges in the Singapore Strait due to winds in the South China Sea

Pavel Tkalich · P. Vethamony · M. T. Babu · Paola Malanotte-Rizzoli

Abstract Among the semi-enclosed basins of the world ocean, the South China Sea (SCS) is unique in its configuration as it lies under the main southwest-northeast pathway of the seasonal monsoons. The northeast (NE) monsoon (November–February) and southwest (SW) monsoon (June–August) dominate the large-scale sea level dynamics of the SCS. Sunda Shelf at the southwest part of SCS tends to amplify Sea Level Anomalies (SLAs) generated by winds over the sea. The entire region, bounded by Gulf of Thailand on the north, Karimata Strait on the south, east cost of Peninsular Malaysia on the west, and break of Sunda Shelf on the east, could experience positive or negative SLAs depending on the wind direction and speed. Strong sea level surges during NE monsoon, if coincide with spring tide, usually lead to coastal floods in the region. To understand the phenomena, we analyzed the wind-driven sea level anomalies focusing on Singapore Strait (SS), laying at the most southwest point of the region. An analysis of Tanjong Pagar tide gauge data in the SS, as well as satellite altimetry and reanalyzed wind in the region, reveals that the wind over central part of SCS is arguably the most important factor determining the observed variability of SLAs at hourly to monthly scales. Climatological SLAs in SS are found to be positive, and of the order of 30 cm during NE monsoon, but negative, and of the order of 20 cm during SW monsoon. The largest anomalies are associated with intensified winds during NE monsoon, with historical highs exceeding 50 cm. At the hourly and daily time-scales, SLA magnitude is correlated with the NE wind speed over central part of SCS with an average time lag of 36–42 h. An exact solution is derived by approximating the elongated SCS shape with one-dimensional two-step channel. The solution is utilized to derive simple model connecting SLAs in SS with the wind speeds over central part of SCS. Due to delay of

P. Tkalich (✉)
Tropical Marine Science Institute, National University of Singapore,
14 Kent Ridge Road, Singapore, Singapore
e-mail: tmspt@nus.edu.sg
URL: www.porl.nus.edu.sg

P. Vethamony · M. T. Babu
National Institute of Oceanography, Dona Paula, Goa 403 004, India

P. Malanotte-Rizzoli
Massachusetts Institute of Technology, 77 Massachusetts Avenue, Cambridge, MA 02139-4307, USA

sea level anomaly in SS with respect to the remote source at SCS, the simplified solutions could be used for storm surge forecast, with a lead time exceeding 1 day.

Abbreviations
SCS   South China Sea
NE   Northeast monsoon
SW   Southwest monsoon
TG   Tanjong Pagar tide gauge
SLA   Sea level anomaly
SS   Singapore Strait

1 Introduction

Storm surges have been an important subject for intensive studies worldwide. Nicholls (2002, 2003) estimated that in the past 200 years, 2.6 million people have drowned during surge events, and taking into consideration the full range of climate change scenarios up to 2100, the death toll could be from 0.4 to 39 million/year. Von Storch and Woth (2008) generalized that in spite of the global scale threat, due to relatively small lateral extent of storm surges, the problem is considered to be a regional, and scientific insights and methods developed for one part of the world do not necessarily find their way into other parts. In particular, they gave an overview of storm surge phenomenon of the North Sea.

Low-laying coastal areas in the South East Asia (SEA) experience disastrous storm surges. According to Dasgupta et al. (2009), out of ten cities that are vulnerable to storm surges, almost half of them are situated in the SEA countries, such as (alphabetically) Bangladesh, China, India, Indonesia, Philippines, Sri Lanka and Vietnam. Along the Bangladesh coast itself, tropical storms of 1876, 1891, 1970 and 1991, and the subsequent surges taken a toll of 100,000 lives (Gönnert et al. 2001). It may also be noted that storm surges in the Bay of Bengal attracted the largest number of publications such as Das (1972), Flierl and Robinson (1972), Murty et al. (1986), Khalil (1992), Vatvani et al. (2000), Rao et al. (2004), Kumar et al. (2008) and Dube et al. (2009).

Storm surges as a separate phenomenon are less studied in the South China Sea (SCS) and Sunda Shelf in particular (Fig. 1a). Vatvani et al. (2000) developed an operational storm surge model encompassing entire SCS with a focus on Vietnam coast. Several studies have been conducted for validating storm surge models for the Gulf of Thailand (Phaksopa and Sojisuporn 2006; Wannawong et al. 2010; Sirisup and Tomkratoke 2010). Sunda Shelf has a typical depth of 100 m, whereas depth at northeast part of SCS exceeds 3,000 m. The uniqueness of sea level anomalies and storm surges over Sunda Shelf is that due to a broad lateral extent of the shallow water domain, the phenomenon could be studied using satellite altimetry data (TOPEX/Poseidon, http://www.aviso.oceanobs.com/duacs/) available daily. Even though satellite data are less accurate in the nearshore than tide gauge records, they have unmatched coverage in the open sea where tide gauges are not installed. Several studies on sea level anomalies have been carried out using altimetry in the SCS in the context of regional scale oceanographic processes (Hwang and

Chen 2000; Shaw et al. 1999; Ho et al. 2000; Liu et al. 2001a, b; Fang et al. 2006; Cheng and Qi 2007; Rong et al. 2007).

The Singapore Strait (SS) is a shallow and narrow water body centrally located at the Sunda Shelf and connected to SCS to the east and the Strait of Malacca to the west (Fig. 1b). The bathymetry of SS is complicated with depth ranging from 20 to 200 m. Several major tidal constituents propagate in the SCS through Luzon Strait, and some
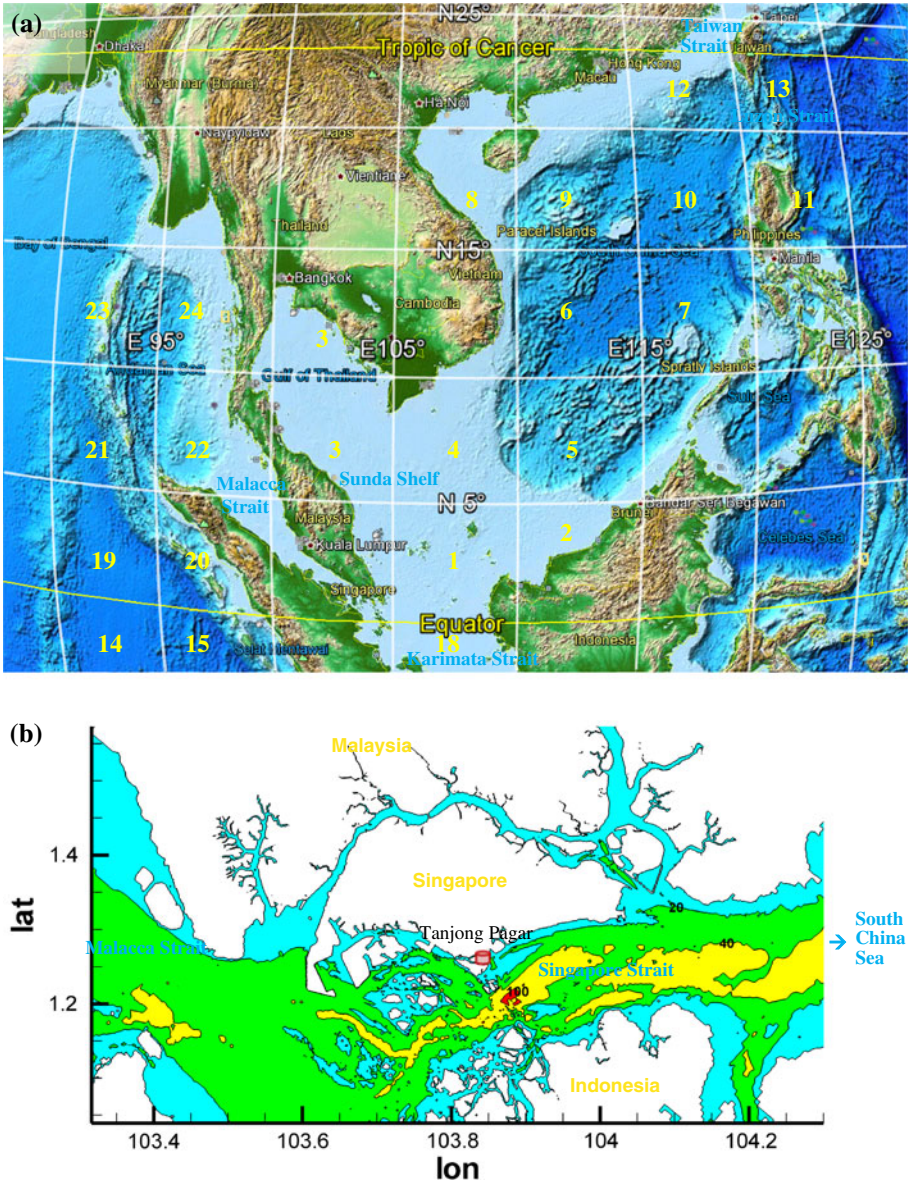

Fig. 1 Regional bathymetry: **a** South China Sea with 5°×5°; **b** Singapore Strait with Tanjong Pagar tide gauge

shallow water components are generated at the adjacent continental shelves—all contributing to a maximum tidal range of about 3 m in the SS. While currents in the SS are predominantly tidal-driven, northeast (NE) winds over SCS enhance the flood (westward) residual flow, and southwest (SW) winds enhance the ebb (eastward) residual flow (Pang and Tkalich 2003; Chan et al. 2006). The wind is causing sea level anomalies, sometimes exceeding 50 cm, positive during NE monsoon and negative during SW monsoon. While these SLAs are not dangerous alone, when coincide with king tides, they can generate widespread coastal floods in the region such as the one happened on 23 December 1999.

In the present study, we show the relation of satellite sea surface anomaly with the wind at a daily to semiannual scale. In the SW monsoon (June–August), the wind is blowing along the axis Singapore–Taiwan, resulting in sea level elevation off Luzon and depression over Sunda Shelf, while during NE monsoon (November–February), the wind changes direction to opposite, causing reversal of the SLA pattern. Even though earlier studies presented correlation of SLA with wind speed at monthly scale, accurate description of storm surge problem requires at least hourly records that could be provided by tide gauges only. We use TOPEX/Poseidon (T/P) satellite altimetry data to understand the formation of sea level anomaly in the SCS in general, and Tanjong Pagar (TG) tide gauge data to quantify the extreme SLAs in the SS in particular. Extreme sea level anomalies (>30 cm) are correlated to large-scale wind patterns over relevant zones of SCS. Simplified solutions are derived to express sea surface height as a function of wind speed, fitted to the available data. Due to delay of sea level anomaly in SS with respect to remote source in the SCS, the expression could be used for forecasting purposes with a lead time of 1–2 days.

2 Data analysis

2.1 Sea level anomalies in the Singapore Strait

To retrieve non-tidal signal due to SLAs for the period 1984–2007, Tanjong Pagar hourly tide gauge data have been subject to harmonic analysis, and 69 constituents have been obtained. Among astronomic principal and major tidal harmonics with amplitudes $M2 = 75.80$ cm, $S2 = 30.02$ cm, $K1 = 29.19$ cm, $O1 = 28.97$ cm, $N2 = 14.69$ cm, $K2 = 8.94$ cm, $P1 = 9.23$ cm, $Q1 = 6.00$ cm, we noted a comparable amplitude of annual $SA = 13.37$ cm and semiannual $SSA = 2.97$ cm constituents, which reflect seasonal meteorological variations influencing the sea level. In our case, the annual and semiannual periods are driven by monsoon cycling between NE and SW. To exclude major influence of local features on TG records, we have compared it with neighboring tide gauges data in SS to find similar patterns (not included in the paper). If we subtract the harmonics from the original tide gauge data, we get residual values qualified as sea level anomalies. We could remove SA and SSA harmonics from the residuals to highlight sea level surges due to specific wind events in the SCS or retain the constituents to observe the anomalies on a back of monsoon-driven surge.

Another source of SLA data are TOPEX/Poseidon sea surface altimetry data available since 1992 (http://apdrc.soest.hawaii.edu) at weekly resolution initially, but refined to daily snapshots eventually. The anomalies are calculated with respect to 7 year mean (January 1993 to December 1999) and mapped on a global irregular grid with 1/3 degree spacing. To represent sea level in SS, the data over 5 degree box centered off Singapore are spatially and weekly averaged and compared with the TG anomalies with SA and SSA included (Fig. 2). Both data sets clearly show seasonal variability of sea level anomalies in the SS:
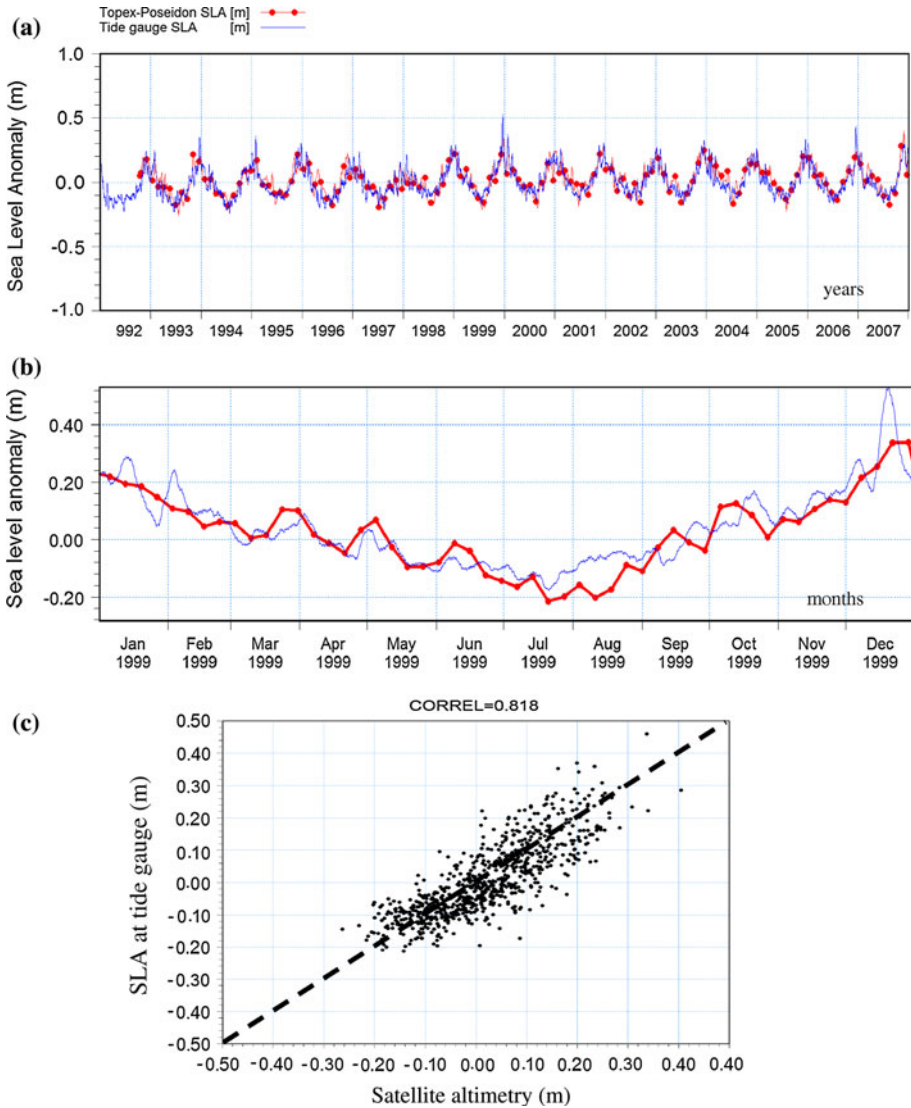
Fig. 2 Sea level anomalies: **a**, **b** derived from Tanjong Pagar tide gauge and satellite altimetry; **c** correlation between tide gauge and satellite altimetry data

positive during NE monsoon, and negative during SW monsoon. In spite of commonly known poor performance of satellite altimetry in coastal regions, the match is surprisingly good with a robust correlation coefficient 0.82. The successful comparison could be possible due to an extensive sea level surges generated over Sunda Shelf by regional wind. Still, as one can expect, the high-resolution tide gauge data show sharper peaks as one sticking out on December 1999. The above analysis ensured cohesiveness of tide gauge data and satellite altimetry, and therefore, we can use latter to track origin of sea level surges over the entire SCS domain.

2.2 Effect of monsoon on SLA

Detailed description of wind system over the SCS is not the primary goal of this work; therefore, readers may refer to the reviews of Wang et al. (2005, 2009) and Chang et al. (2011). It is important to note that monsoon wind is fairly uniform over the SCS, and typhoons are common only at the NE corner of the sea, propagating generally toward Taiwan, China and Vietnam. All major past sea level extremes in SS (partially illustrated in Sect. 2.3) have been generated by monsoon surges, manifested as increase of monsoonal wind above the usual range for a few consecutive days. The affected area usually spans over significant part of the SCS; therefore, satellite altimetry and six-hourly NCEP wind (Kalnay et al. 1996; http://www.esrl.noaa.gov/psd/) have sufficient resolution for the studied phenomenon. For convenience of analysis, we averaged NCEP wind over 5 degree cells, assigned to their centers (as shown in Fig. 1a) and numbered in the text from W1 to W24.

We compare climatologies of altimetry versus gridded NCEP winds for the period 1993–2008 in Fig. 3. The climatological NE and SW wind is aligned roughly along the longest axis of SCS depicted by solid lines, or in more refined terms, along the streamlines depicted by dashed curves having a sharp turn almost 90° at the southernmost tip of the Malay Peninsula. Ends of the curves rest on the cell W9, representing area offshore of Vietnam and Hainan Island from one side, and cell W18 corresponding to Karimata Strait from another side. The climatological wind along the streamlines is the strongest off Vietnam and the weakest over Karimata Strait. More information on wind speed and direction could be obtained from wind-rose diagrams depicted in Fig. 4. While 6-hourly wind off Vietnam may exceed 15 m/s quite frequently, wind over Karimata Strait does not reach 8 m/s. Six-hourly wind speed at cell W9 may even exceed the threshold of 17.5 m/s, established by NOAA for 1-min-average wind to be classified as a tropical storm. Figure 5a, b shows wind and SLA climatologies for the period 1993–2008 along the cross-section Taiwan–Singapore, while Fig. 5c depicts the bottom profile. Figure 5a illustrates the climatological wind speeds for the NE and SW monsoons. The strongest NE wind is measured at two areas, one off Taiwan and another off Vietnam shores (near geographical center of SCS); strongest SW wind has one peak off Vietnam. The climatological wind at the center of SCS seems to drive SLA toward Taiwan during SW monsoon, or toward Sunda Shelf during NE monsoon. Figure 5b shows the corresponding climatological SLAs exceeding 10 cm over the Sunda Shelf, positive during NE monsoon and negative during SW monsoon. Interestingly, several nodal points of sea level are found to be aligned above sharp gradients of the bottom profile, out of which we note the one at the center of the cross-section corresponding to the bottom drop exceeding 2,000 m. The phenomenon will be investigated in Sect. 3.1 using an analytical solution.

SLA variability with respect to the driving wind is analyzed further. The frequency distribution of hourly SLA time series at different months throughout a year is presented in Fig. 6. It is somewhat positively skewed during the NE monsoon, and to a lesser degree negatively skewed during the SW monsoon, but otherwise near symmetrical around floating mean value, positive during NE and negative during SW monsoon. While December and March see wider variability of anomalies, the frequency distribution during other periods is fairly centralized with the dispersion of about 20 cm. Figure 7 shows annual distribution of SLAs in SS reflecting regional climate signals, such as ENSO. In particular, stronger positive skewness is observed during El Niño and La Niña episodes, with the mean sea level dipping during El Niño episodes of 1987–1988 and 1991–1992, but elevated above average during La Niña episodes of 1988–1989 and 1999–2000. In other
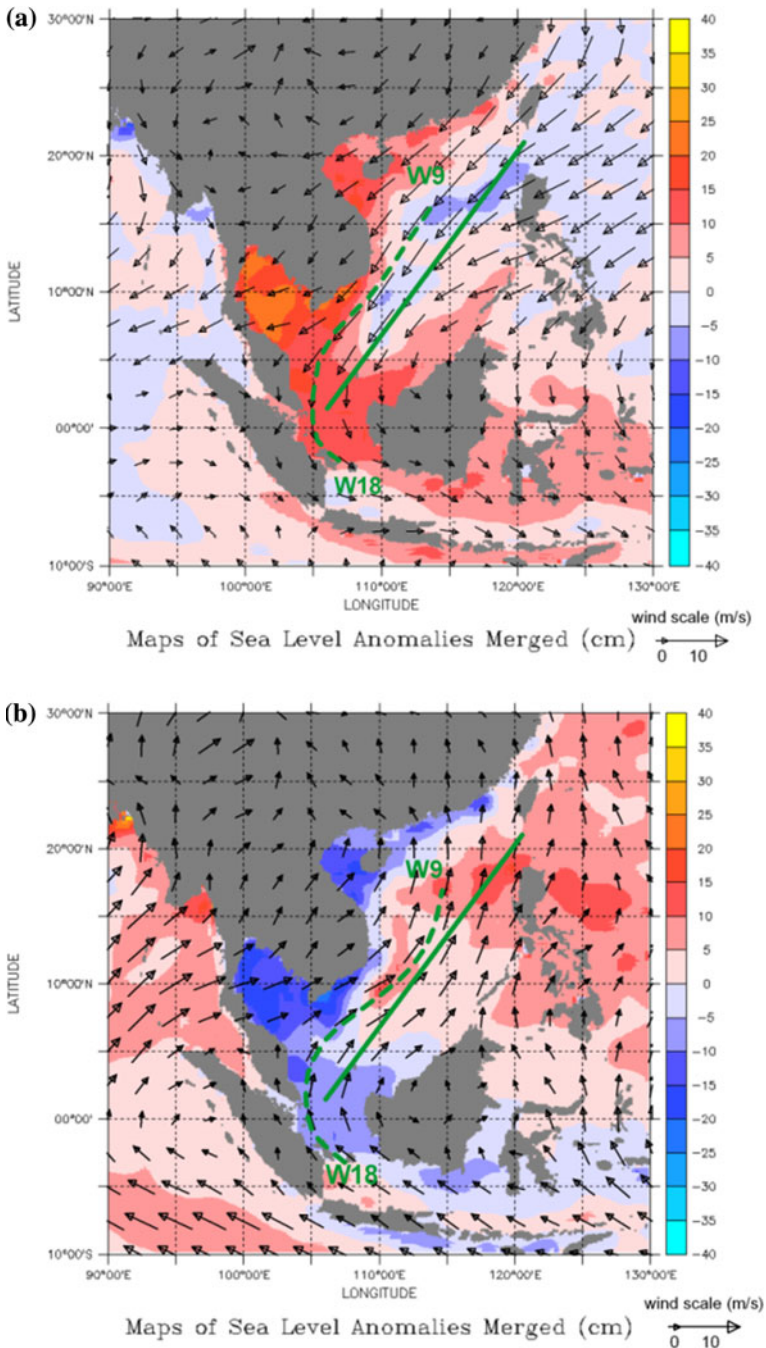
Fig. 3 Climatological seasonal 6-hourly wind and satellite altimetry averaged over 1993–2008 years: **a** NE Monsoon (November–February), **b** SW Monsoon (June–August). *Solid line* is the longest axis of Taiwan–Singapore, and *dash-lines* are the wind speed streamlines
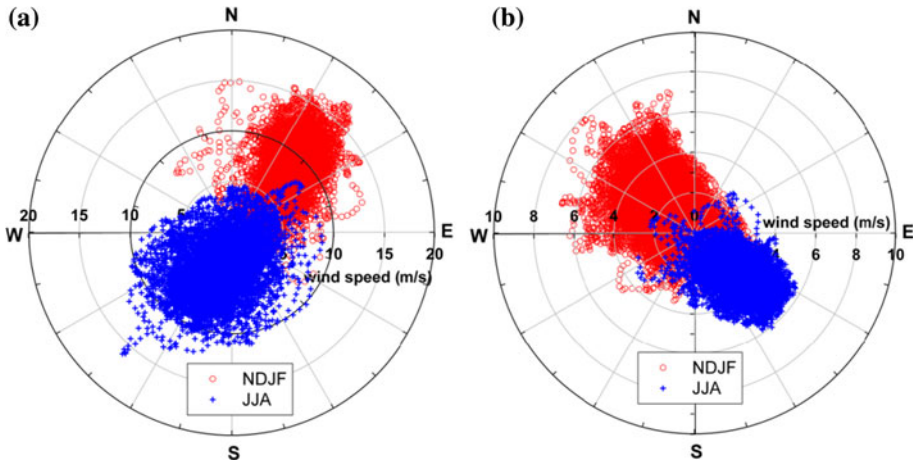
Fig. 4 Climatological wind-rose diagrams for the period 1984–2007 at wind cells (Fig. 1a): **a** wind cell W9 (off Vietnam), **b** wind cell W18 (Karimata Strait). NE monsoon wind is depicted by *red circles*, while SW monsoon wind is shown by *blue crosses*
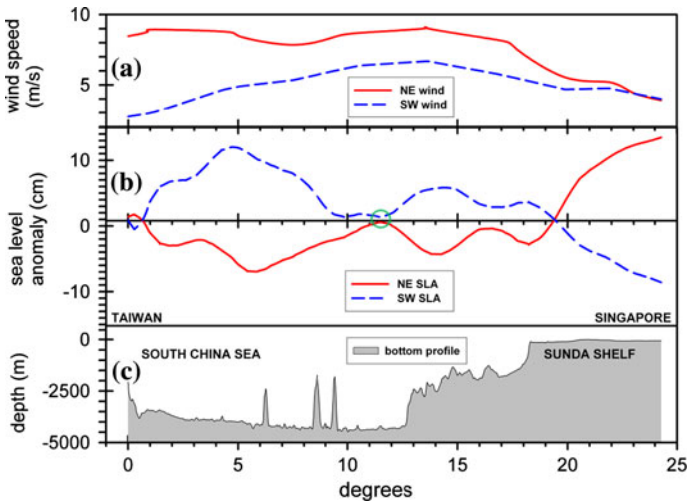

Fig. 5 Cross-section of the South China Sea from Taiwan to Singapore Strait as shown by solid lines in Fig. 3: **a**, **b** climatological wind and sea level anomalies for the period 1993–2008; **c** bottom profile. A nodal point at seasonal sea level is shown by a *circle*

years, the annual frequency distribution may show two peaks corresponding to NE and SW monsoons.

2.3 Correlation of SLA with gridded regional wind

In the original TG data (even before detiding), some extremes are sticking out when high sea level cases coincide with the spring tide, usually during NE monsoon. For illustrative purpose, we have selected several cases exceeding a threshold value 3.3 m above Chart
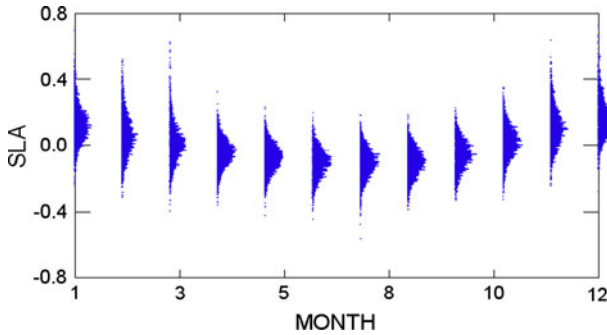
Fig. 6 Monthly frequency distribution of SLAs for the period 1984–2007
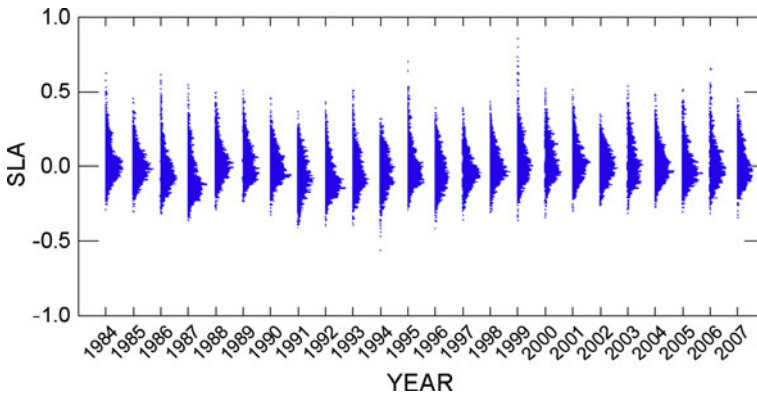

Fig. 7 Annual frequency distribution of SLAs

Datum (corresponding to Highest Astronomic Tide) and drawn up maps of satellite anomalies overlapped with NCEP wind (Fig. 8). We could observe qualitatively similar phenomenon for all the cases, where strong wind blows along the axis of Taiwan–Singapore, rising sea level over the entire Sunda Shelf. One of the most extreme events in the recent history (22–23 December 1999) caused widespread floods in the region.

From the above analysis, we noted that extreme SLAs derived from tide gauge data in the SS are lagging by about 1 day behind the strong wind over central part of SCS and massive surge at Sunda Shelf. In order to enumerate the dependence, we correlated extreme SLAs with gridded NCEP wind (Fig. 1a). For correlation analysis, only one maximum SLA of a year that exceeds the threshold value of 30 cm (if any) is selected. As we are dealing with a daily-scale surge phenomenon, we have removed the annual (SA) and semi-annual (SSA) "monsoon" components from the tide record. Statistical analysis (Table 1) shows correlation of surges in the SS with wind speeds at the 5 degree grid with a time lag indicated in brackets by number of 6-hourly intervals. We could observe clearly that for the NE monsoon, the time lag is approximately proportional to the distance between the specific wind cell and SS. The time lag also depends on the cell position, that is whether it is embedded in or nearby coastal features (as cell W8) or it is located in the open sea along the longest axis (similar to cells W4–W7, W9–W10). The lags during the SW monsoon are rather irregular, due to the fact that SS is situated at the rear (weak) part
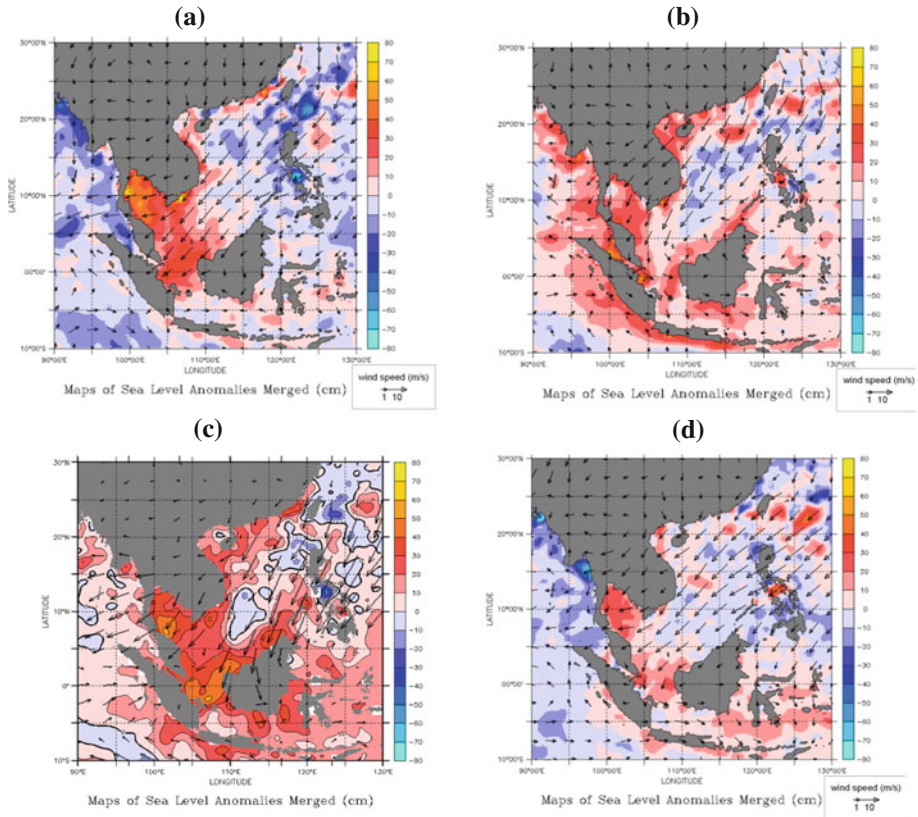
Fig. 8 Selected extremes of sea level anomalies overlapped with corresponding wind. **a** February 1, 1995, **b** November 24, 1995, **c** December 22, 1999, **d** March 8, 2004

of wind system during this period. The most prominent result emerging from the correlation analysis is that the surges in SS are all positively correlated with the wind during NE monsoon and negatively correlated with the one during SW monsoon.

It is clear from Table 1 that SLAs in SS and wind cells W6, W9 and W10 have highest correlations, varying from 0.514 to 0. 541 with an average time lag of about 36–42 h. In absolute terms, the correlation does not look particularly high, possibly due to the following reasons: (1) correlation coefficient is a measure of the strength of the linear relationship between two variables, which is less accurate for a nonlinear relationship between wind speed and surge height (as will be found in Sect. 3); and (2) atmospheric force is applied over a large area of SCS and distributed at a distance over 1,000 km from SS; therefore, no particular small area is directly responsible for remote surges. The dependence and time delay could be illustrated using time series of wind speed and direction off Vietnam (W9) and daily averaged SLA for extreme cases on 25 November 1995 and 23 December 1999 (Figs. 9, 10, respectively). In both the cases, the peaks of SLAs are following the wind speed peaks with a time lag about 1 day.

Among wind cells south of Singapore, as one might expect, only the wind over Karimata Strait (W18) has some noticeable correlation and a short time lag. Analysis of wind streamlines sketched in Fig. 3a, b offers explanation to these phenomena as the SS

Table 1 Cross correlation between wind speed and SLA at 18 selected NCEP wind areas in the SCS, Singapore Strait and Bay of Bengal, during the NE monsoon period (November–February) and SW monsoon period (June–August)

NCEP wind grid location Latitude (N): longitude (E)		Cross correlation and (lag in 6 h intervals)	
		Wind speed versus SLA (November–February)	Wind speed versus SLA (June–August)
W1	00–05N:105–110E	0.361 (0)	−0.31 (0)
W2	00–05N:110–115E	0.218 (6)	−0.15 (7)
W3	05–10N:100–105E	0.494 (5)	−0.10 (5)
W4	05–10N:105–110E	0.373 (5)	−0.24 (5)
W5	05–10N:110–115E	0.371 (5)	−0.22 (7)
W6	10–15N:110–115E	0.514 (6)	−0.25 (4)
W7	10–15N:115–120E	0.416 (5)	−0.19 (5)
W8	15–20N:105–110E	0.441 (9)	−0.09 (1)
W9	15–20N:110–115E	0.541 (6)	0.09 (−1)
W10	15–20N:115–120E	0.523 (7)	−0.15 (4)
W11	15–20N:120–125E	0.459 (5)	−0.08 (7)
W12	20–25N:115–120E	0.428 (9)	−0.10 (5)
W13	20–25N:120–125E	0.337 (7)	−0.07 (7)
W14	05S–0N:090–095E	0.04 (4)	−0.15 (2)
W15	05S–0N:095–100E	0.01 (−1)	−0.12 (−4)
W16	10S–05S:090–95E	0.13 (−25)	−0.12 (−17)
W17	10S–05S:095–100E	0.11 (−23)	−0.11 (−8)
W18	05S–0N:105–110E	0.20 (−4)	−0.19 (−4)

being "sandwiched" between winds at cells W9 and W18, with W9 dominating due to a stronger intensity and longer fetch. All other wind cells are obstructed by land masses, fully or partially; therefore, the influence of the wind on SS surges is smaller.

3 Simplified solutions for storm surges in SCS

The above analysis has shown that seasonal and extreme winds, their persistence, intensity and direction play a primary role in forcing sea level surges in the Sunda Shelf, in general, and SS, in particular. The finding encouraged us to seek a simplified solution relating height of sea level surges in SS with the wind speed in SCS. If successful, such relationship could serve as a simple and quick forecasting tool of sea level extremes in SS.

3.1 1-D Analytical model for SCS

It has been identified that the NE (SW) monsoon climatological and extreme wind, when aligned along the longest axis of SCS Taiwan–Singapore, produces the strongest positive (negative) sea level surges in SS. According to the phenomenological description, one can simplify the sea level surge generation problem in SCS using a rectangular domain, with the longest axis parallel to the direction of the NE/SW monsoon (Fig. 11a). In Malanotte-Rizzoli (2011), a rather complex analytical treatment was developed to elucidate the dynamics of the steady-state set-up under the forcing wind, and the free oscillations of the
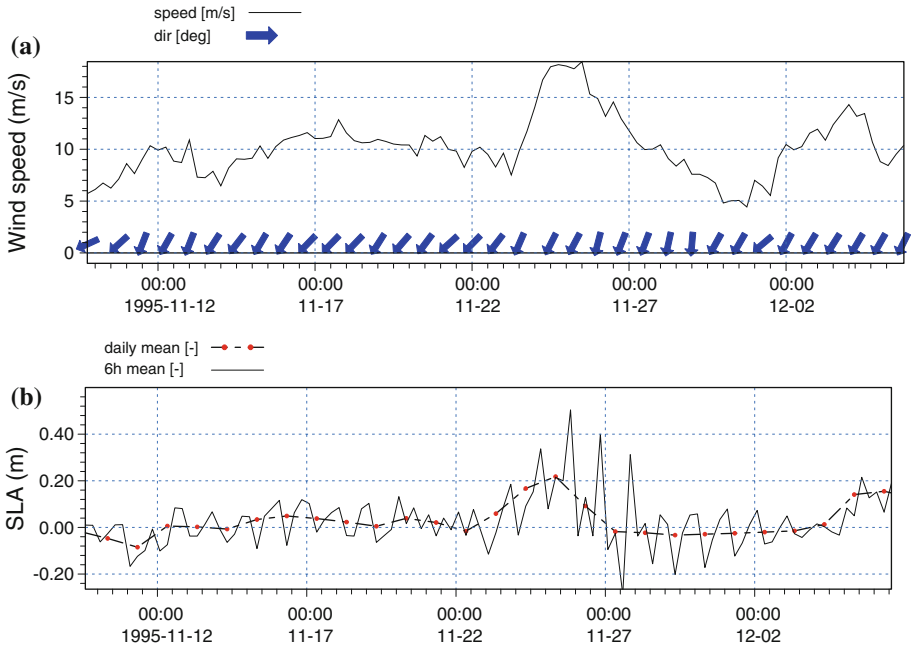
Fig. 9 a NCEP wind speed and direction at 12.5°N and 112.5°E, **b** sea level anomaly at Tanjong Pagar during the highest spring tide of November 25, 1995
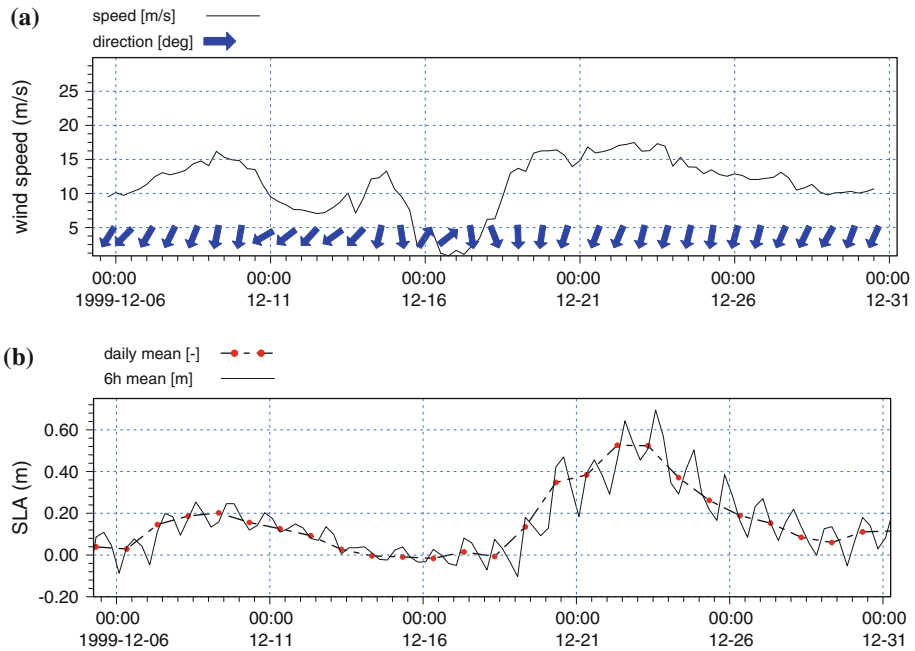

Fig. 10 a NCEP wind speed and direction at 15°N and 110°E, **b** extreme sea level anomaly (without annual and semi-annual components) at Tanjong Pagar during the highest spring tide of December 23, 1999
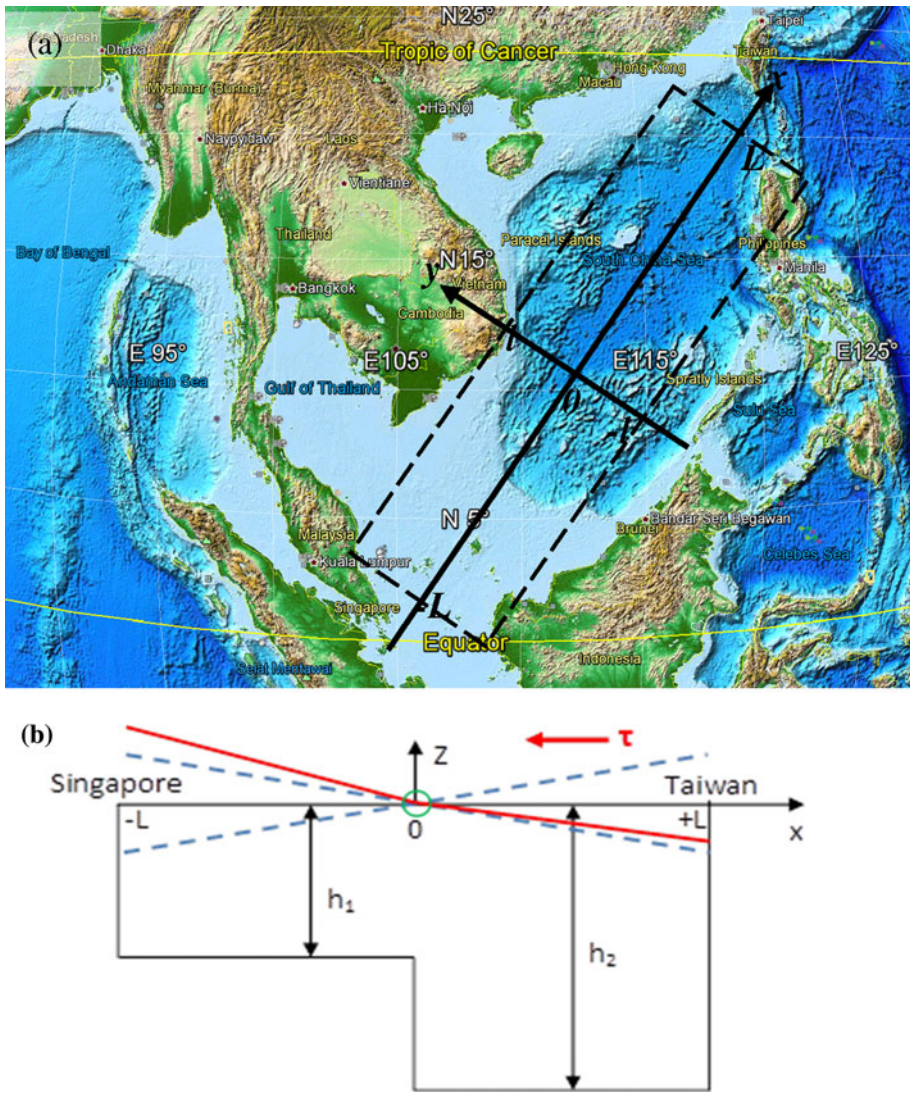
Fig. 11 Conceptual model of storm surges in a channel: **a** 2-D case, **b** 1-D model of the steady-state set-up (solid red line) and free oscillations (dashes gray lines) along the main axis of the SCS shown in Fig. 5 during the northeast monsoon. Nodal point over shelf break is shown by a *circle*

basin superimposed to the steady solution. Because of the width of the SCS, rotation cannot be assumed a priori negligible. Hence, the two-dimensional linear shallow water equations with constant rotation in a closed rectangular basin with constant depth are considered under wind stress forcing. One-dimensional analysis is carried out following Pedlosky (2003, Chap. 14). In a suitable parameter range, the resulting equation for sea level is the wind stress forced equivalent of Pedlosky's Eq. (14.24). This equation can be further simplified by assuming uniformity of sea level and wind stress in cross-basin (y) direction, idealizing the sea level response under the monsoon system. The resulting analytical solution consists of opposite steady-state set-up at the two ends of the basin

under the wind blowing along the main axis, with superimposed two oppositely traveling waves. The boundary conditions at the two-end side walls give rise to a standing wave, the seiche. The solution, even though approximate, elucidates the role of rotation, which produces a rotation-dependent modulation of both the steady and wave components. Then, the further approximation can be made considering a one-dimensional configuration without rotation.

The one-dimensional channel configuration is depicted in Fig. 11b with the Sunda Shelf extending from $x = -L$ (Singapore) to the center of the basin $x = 0$ and depth h_1; the deep interior extending from $x = 0$ to $x = +L$ (Taiwan) and depth h_2; and a step-like continental slope separating them. We do not solve the transient problem of a sudden wind onset and relaxation with consequent excitation of the seiche. Rather, we solve for the background, steady set-up on which free oscillations are superimposed whose wavelengths are discretized by the side walls boundary conditions.

The one-dimensional shallow water equations for the depth-independent along channel velocity u and the sea level η are:

$$\frac{\partial u}{\partial t} = -g\frac{\partial \eta}{\partial x} + \frac{\tau}{\rho_0 h}$$
$$\frac{\partial \eta}{\partial t} + h\frac{\partial u}{\partial x} = 0 \tag{1}$$

where, ρ_0 is the water density. Equation (1) could be rewritten as

$$\frac{\partial^2 u}{\partial t^2} - gh\frac{\partial^2 u}{\partial x^2} = \frac{\partial}{\partial t}\left(\frac{\tau}{\rho_0 h}\right)$$
$$\frac{\partial^2 \eta}{\partial t^2} - gh\frac{\partial^2 \eta}{\partial x^2} = -h\frac{\partial}{\partial x}\left(\frac{\tau}{\rho_0 h}\right) \tag{2}$$

having steady-state solution (apart from an arbitrary time-dependent integration function for η):

$$\eta_s = \frac{1}{\rho_0 gh}\int \tau dx$$
$$u_s = -\frac{1}{2\rho_0 gh^2}\frac{\partial \tau}{\partial t}x^2 + Ax + B \tag{3}$$

Existence of sea level node over the edge of the shelf break is supported by observations in Fig. 5b; therefore, in the simplified case depicted in Fig. 11b, we specialize to regions (1) and (2) with depths (h_1, h_2) respectively and require that the origin be a sea level node, i.e.

$$\eta_1 = \eta_2 = 0 \quad \text{at } x = 0.$$

If the wind stress is constant in x, the solutions for the steady-state set-up can be written as, apart again from an arbitrary time-dependent integration function:

$$\eta_{s1} = \frac{1}{\rho_0 gh_1}\ \tau x$$
$$\eta_{s2} = \frac{1}{\rho_0 gh_2}\ \tau x \tag{4}$$

showing that the sea level response under a wind blowing in the $(-x)$ direction (NE monsoon) is higher on the shelf (at $x = -L$, Singapore) because of the shallow depth, and

the corresponding depression at $x = +L$ (Taiwan) is smaller because of the deep basin. Notice that while the steady-state sea level is continuous at $x = 0$, its slope is not.

Further requiring that $\eta = 0$ at initial time $t = 0$, the wave solution to the homogeneous Eq. (2) for the sea level at the two basins is:

$$\eta_{w1} = a\sin(k_1\sqrt{gh_1}t)$$
$$\eta_{w2} = a\sin(k_2\sqrt{gh_2}t)$$

(5)

This wave solution satisfies the two conditions of being zero at $x = 0$ and at initial time $t = 0$.

The wave numbers k_1 and k_2 are found imposing the boundary conditions at the two side walls $x = -L$ and $x = +L$. Imposing for instance maximum/minimum elevations:

$$\sin(k_1 L) = -1 \quad \text{at } x = -L$$
$$\sin(k_2 L) = -1 \quad \text{at } x = +L$$

gives $k_1 = k_2 = (3\pi/2 + 2\pi n)/L$ with $n = 1, 2,\ldots$, as the two basins have equal widths. Hence, for the free wave, also the slope is continuous at $x = 0$.

We do not present here the solutions for the velocities as in (Malanotte-Rizzoli 2011). Again, the integration constants are found by imposing the boundary conditions at the two side walls and the matching conditions at $x = 0$ where continuity of transport is required. Velocities are discontinuous at $x = 0$. A continuous solution might have been found by specifying an analytical shape for the continental slope. However, the analytical solution, when obtainable, would be much more complex without adding anything to the dynamics.

3.2 Simplified model for storm surges in Singapore Strait

The basic result of the above analytical model (Eq. 4) is that the steady-state sea level set-up is linearly dependent on the wind shear stress as

$$\eta = \frac{1}{\rho_0 g h}\tau x$$

(6)

Here, the wind shear stress is given by

$$\tau = C_d \rho_a W^2$$

(7)

where C_d is the drag coefficient, ρ_a the density of air, and W is the wind speed at 10 m.

We want to explore how well the simple model, Eqs. (6)–(7), performs for storm surges over Sunda Shelf including SS during NE monsoon. Typical values for Sunda Shelf could be taken as follows: fetch $x = 1,000$ km, depth $h = 100$ m; and rest parameters are not site specific, namely $\rho_a = 1.25$ kg/m^3, $\rho_0 = 1,025$ kg/m^3, and $g = 9.81$ m/s^2. While the best approximation for the drag coefficient is still discussed, for illustrative purpose, we use simple and yet versatile expression by Wu (1982)

$$C_d = 10^{-3}(0.8 + 0.065W)$$

(8)

In Fig. 12, we plot together SLAs in SS versus wind speed at cell W9 for all NE monsoons during period 1984–2007, and the exact solution Eqs. (6)–(8) with the specified parameters. There is a good agreement between the data and the model, indicating that SLAs in SS are indeed driven by storm surges in SCS. There is also confidence that the simple model, Eqs. (6)–(8), may serve as a quick assessment of storm surges in SS using forecasted wind speed offshore of Vietnam.
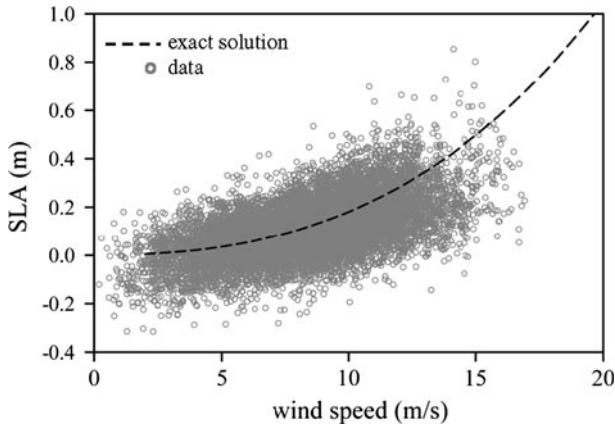
Fig. 12 Storm surge height in Singapore Strait versus wind speed. *Dots* are SLAs from tide gauge in Singapore Strait vs wind at cell W9. *Line* is the exact solution, Eqs. (6)–(8)

4 Conclusions

Among the semi-enclosed basins of the world ocean, the South China Sea is unique in its configuration as it lies under the main southwest-northeast pathway of the seasonal monsoons. The NE monsoon (November–February) and SW monsoon (June–August) dominate the large-scale sea level dynamics of the SCS. Sunda Shelf at SW part of SCS tends to amplify Sea Level Anomalies (SLAs) generated by wind over the sea. The entire region, bounded by Gulf of Thailand on the north, Karimata Strait on the south, east cost of Peninsular Malaysia on the west, and break of Sunda Shelf on the east, could experience positive or negative SLAs depending on the wind direction and speed. Strong sea level surges during NE monsoon, if coincide with spring tide, usually lead to coastal floods in the region.

To understand the phenomena, we analyzed sea level anomalies focusing on SS, laying at the most SW point of the region. An analysis of Tanjong Pagar tide gauge data in the SS, as well as satellite altimetry and reanalyzed wind in the region, revealed that the wind over central part of SCS is arguably the most important factor determining the observed variability of SLAs at hourly to monthly scales. Climatological SLAs at SS are found positive, and of the order of 30 cm during NE monsoon, but negative, and of the order of 20 cm during SW monsoon. The largest anomalies are associated with intensified winds during NE monsoon, with historical highs exceeding 50 cm. At the hourly and daily time-scales, SLA magnitude is correlated with the NE wind speed over central part of SCS with an average time lag of 36–42 h.

An exact solution is derived by representing the elongated SCS shape with one-dimensional two-step channel. The solution is utilized to derive a simple model connecting SLA in SS with the wind speed over central part of SCS. Due to delay of sea level anomaly in SS with respect to the remote source at SCS, the simplified solution could be used for storm surge forecast with a lead time exceeding 1 day.

References

AVISO site: http://apdrc.soest.hawaii.edu

Chan ES, Tkalich P, Gin K, Obbard J (2006) The physical oceanography of Singapore coastal waters and its implications for oil spills. In: Wolanski E (ed) The environment in Asia Pacific harbours. Springer, New York, pp 393–412

Chang CP, Ding Y, Lau NC, Johnson RH, Wang B, Yasunari T (2011) The global monsoon system: research and forecast, 2nd edn. World Scientific Publishing, Singapore, p 608, ISBN-10: 9814343404

Cheng X, Qi Y (2007) Trends of sea level variations in the South China Sea from merged altimetry data. Glob Planet Chang 57:371–382

Das PK (1972) Prediction model for storm surges in the Bay of Bengal. Nature 239:211–213

Dasgupta S, Laplante B, Murray S, Wheeler D (2009) Climate change and the future impacts of storm-surge disasters in developing countries—working paper 182, http://www.cgdev.org/files/1422836_file_Future_ Storm_Surge_Disasters_FINAL.pdf

Dube SK, Jain I, Rao AD, Murty TS (2009) Storm surge modelling for the Bay of Bengal and Arabian Sea. Nat Hazards 51:3–27. doi:10.1007/s11069-009-9397-9

Fang G, Chen H, Wei Z, Wang Y, Wang X, Li C (2006) Trends and interannual variability of the South China Sea surface winds, surface height, and surface temperature in the recent decade. J Geophys Res 111:C11S16

Flierl GR, Robinson AR (1972) Deadly surges in the Bay of Bengal: dynamics and storm tide tables. Nature 239:213–215

Gönnert G, Dube SK, Murty T, Siefert W (2001) Global storm surges. Die Küste 63:623

Ho CR, Zheng Q, Soong YS, Kou NJ, Hu JH (2000) Seasonal variability of sea surface height in the South China Sea observed with TOPEX/POSEIDON altimeter data. J Geophys Res 105:13981–13990

Hwang C, Chen SA (2000) Fourier and wavelet analyses of TOPEX/Poseidon-derived sea level anomaly over the South China Sea: a contribution to the South China Sea Monsoon experiment. J Geophys Res 105:28785–28804

Kalnay E et al (1996) The NCEP/NCAR reanalysis 40-year project. Bull Am Meteorol Soc 77:437–471

Khalil GM (1992) Cyclones and storm surges in Bangladesh: some mitigative measures. Nat Hazards 6:11–24

Kumar VS, Babu VR, Babu MT, Dhinakaran G, Rajamanickam GV (2008) Assessment of storm surge disaster potential for the Andaman Islands. J Coast Res 24(2B):171–177. doi:10.2112/05-0506.1

Liu Q, Jia Y, Wang X, Yang H (2001a) On the annual cycle characteristics of the sea surface height in the South China Sea. Adv Atmos Sci 18:613–622

Liu Z, Yang H, Liu Q (2001b) Regional dynamics of seasonal variability in the South China Sea. J Phys Oceanogr 31:272–284

Malanotte-Rizzoli P (2011) An analytical model for sea level set-up and seiche response in semi-enclosed basins. MIT internal report, p 9

Murty TS, Flather RA, Henry RF (1986) The storm surge problem in the Bay of Bengal. Proc Oceanogr 16:195–233

Nicholls RJ (2002) Analysis of global impacts of sea-level rise: a case study of flooding. Phys Chem Earth 27:1455–1466

Nicholls RJ (2003) An expert assessment of storm surge "Hotspots". Final report (draft version) to Center for Hazards and Risk Research, Lamont-Dohert Observatory, Columbia University

Pang WC, Tkalich P (2003) Modeling tidal and monsoon driven currents in the Singapore Strait. Singap Marit Port J 151–162

Pedlosky J (2003) Waves in the ocean and atmosphere. Introduction to wave dynamics. Springer, New York, p 260. ISBN 3-540-00340-1

Phaksopa J, Sojisuporn P (2006) Storm surge in the Gulf of Thailand generated by Typhoon Linda in 1997 using Princeton ocean model. Kasetsart J (Nat Sci) 40:260–268

Rao AD, Babu SV, Dube SK (2004) Impact of a tropical cyclone on coastal upwelling processes. Nat Hazards 31:415–435

Rong Z, Liu Y, Zong H, Cheng Y (2007) Interannual sea level variability in the South China Sea and its response to ENSO. Glob Planet Chang 55:257–272

Shaw PT, Chao SY, Fu LL (1999) Sea surface height variations in the South China Sea from satellite altimetry. Oceanol Acta 22:1–17

Sirisup and Tomkratoke (2010) A Scenario-based investigation of storm surge in Thai Gulf: a simulation with finite volume coastal ocean model. Storm Surges Congress, Hamburg, Germany, 13–17 Sept 2010, SSC2010-34-1

Vatvani D, Goodchild S, Stelling GS, Gerritsen H, Van Holland G, Hulsen L, Van Der Kaaij T, Rao AVRK (2000) Storm surge models for Bay of Bengal—India and Vietnam. In: Proceedings of the RTC conference on TC and storm surges, Chiang Mai, Thailand

von Storch H, Woth K (2008) Storm surges: perspectives and options. Sustain Sci 3:33–43. doi:10.1007/s11625-008-0044-2

Wang P, Clemens S, Beaufort L, Braconnot P, Ganssen G, Jian Z, Sarnthein KPM (2005) Evolution and variability of the Asian monsoon system: state of the art and outstanding issues. Quatern Sci Rev 24:595–629

Wang B, Huang F, Wu Z, Yang J, Fua X, Kikuchia K (2009) Multi-scale climate variability of the South China Sea monsoon: a review. Dyn Atmos Oceans 47:15–37

Wannawong W, Humphries UW, Wongwises P, Vongvisessomjai S, Lueangaram W (2010) Numerical modeling and computation of storm surge for primitive equation by hydrodynamic model. Thai J Math 8:355–371

Wu J (1982) Wind-stress coefficients over sea surface from breeze to hurricane. J Geophys Res 87:9704–9706